Electronic Supplementary Material (ESI) for Reaction Chemistry & Engineering.

Supplemental Information belonging to

Analysis of the Propoxylation of Zinc-Cobalt Double Metal Cyanide Catalysts with different active Surfaces and Particles Sizes

Sarah-Franziska Stahl and Gerrit A. Luinstra*

University of Hamburg, Institute for Technical and Macromolecular Chemistry, Bundesstr. 45, 20146 Hamburg, Germany

Supporting Catalyst descriptions

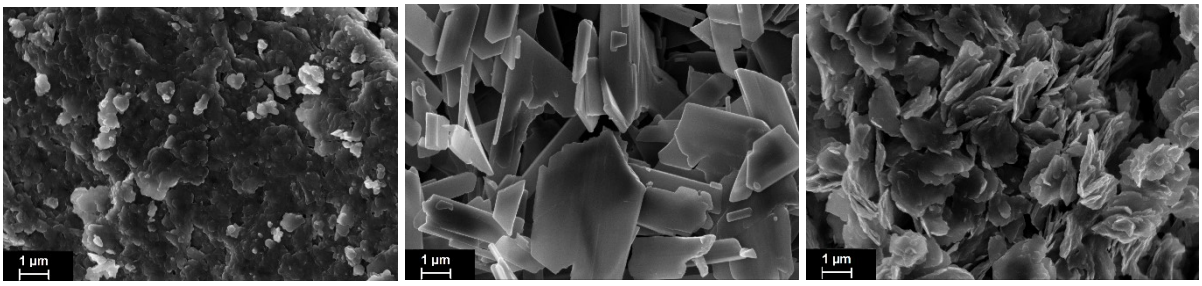

Figure S1 SEM images with 20 000 magnitude of DMC A (l), DMC B (m) and DMC C (r) after thermal treatment (80 °C, 2 h).

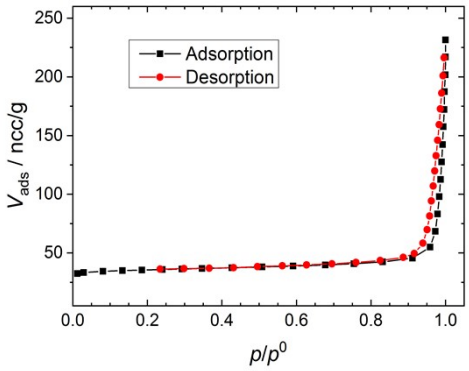

Figure S2 Isotherm of DMC A resulted by adsorption measurements with nitrogen.

DMC complexes are based upon $[M[M'(CN)_6]$ frameworks (here M = Zn^{2+}, M' = Co^{3+}) in which octahedral $[M'(CN)_6]^{n-}$ complexes are linked by M^{n+} ions coordinated to nitrogen atom of the cyanides [1], [2]. The major, sharp reflexes of cubic and presumed catalytically inactive $Zn_3[Co(CN)_6]_2$ at 2θ = 17.0, 23.7, 24.7, 34.3 and 39.9° are found in the XRD of DMC B. DMC A and C show more broadened peaks, obviously on account of the smaller crystallite size, both showing a sharp reflex at 2θ of 23.7° [3]. The XRD pattern of DMC C is consistent with the usual cubic Prussian blue structure type, but intensity and shape of the peaks indicate that parts of the framework have collapsed [4]. The XRD pattern of DMC A shows a resemblance to reported dimorphic cubic and hexagonal structures, in which the zinc metal (M) is octahedral respectively tetrahedral coordinated as it shows considerable reflexes at 2θ = 9.9 and 14.4°, belonging to a semi-crystalline $Zn_3[Co(CN)_6]$ phase [3]. The reflexes at 2θ of 11.3, 16.5 and 21.7° can be assigned to a hexagonal phase (Zn_3Co_2-H) [5], [6].

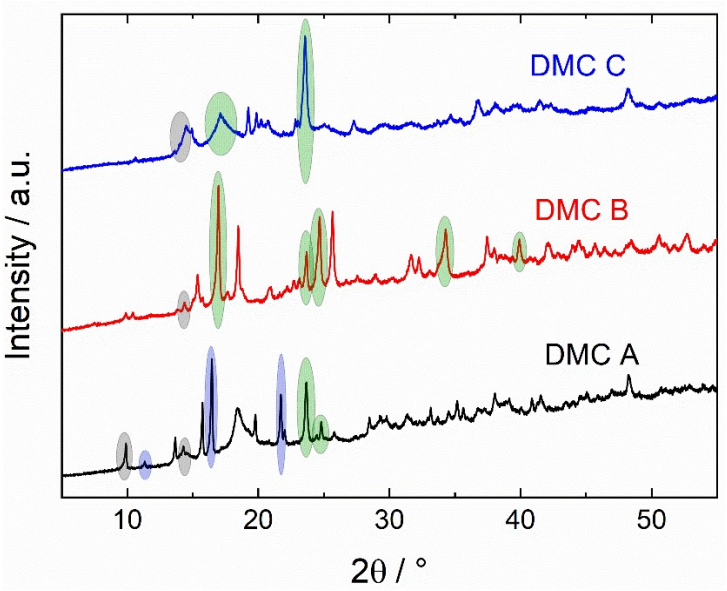

Figure S3 XRD patterns of the catalysts. Reflexes of cubic $Zn_3[Co(CN)_6]_2$ (green), semi-crystalline $Zn_3[Co(CN)_6]$ (grey) and hexagonal Zn_3Co_2-H (blue) are highlighted.

Reaction profile and experimental data in pulse-decay experiments

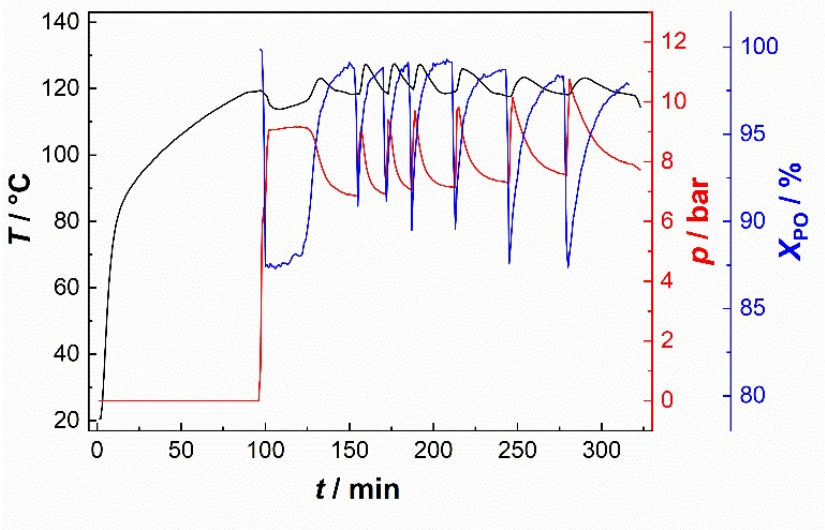

Figure S4 Temperature- and pressure profiles and conversion of PO during pulse-decay experiment including drying procedure, activation phase and pulsed PO additions.

Table S1 Parameters and determined reaction rates of all feeding-step experiments with DMC A.

Nr.	k_{obs} / 10^{-3} · [1/s]	[DMC] / mg/L	[ROH] / mol/L	k_s·K / 10^{-4} · $L^2/(s \cdot mg_{DMC} \cdot mol)$	T / °C
1	4.33 ± 0.23	23.87	0.79	2.29	123.6 ± 4.0
1	3.84 ± 0.15	21.30	0.71	2.55	124.8 ± 3.4
1	3.33 ± 0.11	19.27	0.64	2.70	124.7 ± 2.5
1	1.98 ± 0.17	17.21	0.57	2.01	123.9 ± 2.3
1	1.56 ± 0.04	15.52	0.52	1.95	121.9 ± 1.8
1	1.05 ± 0.02	14.00	0.46	1.61	121.7 ± 1.4
2	8.47 ± 0.22	26.48	0.78	4.08	125.9 ± 4.5
2	8.00 ± 0.18	23.85	0.71	4.75	126.6 ± 4.0
2	6.56 ± 0.04	21.45	0.64	4.81	128.2 ± 2.3
2	4.08 ± 0.12	19.32	0.57	3.69	124.4 ± 3.5
2	2.36 ± 0.02	17.28	0.51	2.67	123.6 ± 2.4
2	1.59 ± 0.02	15.53	0.46	2.23	121.8 ± 2.1
2	1.14 ± 0.02	13.92	0.41	1.98	122.5 ± 2.0
3	5.85 ± 0.17	23.97	0.80	3.07	124.3 ± 3.6
3	4.99 ± 0.12	21.56	0.72	3.24	124.1 ± 2.1
3	3.29 ± 0.05	19.17	0.64	2.70	118.9 ± 1.3
3	1.62 ± 0.06	15.39	0.51	2.06	120.3 ± 1.5
3	1.35 ± 0.02	13.72	0.46	2.16	121.4 ± 2.8
3	0.58 ± 0.02	12.22	0.41	1.02	115.0 ± 2.8
4	2.98 ± 0.10	24.81	0.79	1.52	116.8 ± 0.7
4	2.75 ± 0.10	22.32	0.71	1.73	117.9 ± 1.3
4	2.43 ± 0.07	19.89	0.63	1.93	117.9 ± 1.8
4	1.67 ± 0.04	17.88	0.57	1.63	117.2 ± 0.7
4	0.98 ± 0.02	16.09	0.51	1.19	115.2 ± 0.8
4	0.68 ± 0.01	15.19	0.49	0.92	115.5 ± 1.6
5	1.98 ± 0.04	23.61	0.78	1.07	113.6 ± 0.7
5	1.65 ± 0.02	21.18	0.70	1.11	111.5 ± 1.8

5	1.39 ± 0.01	19.10	0.63	1.14	111.7 ± 3.4
5	1.32 ± 0.06	17.14	0.57	1.35	115.7 ± 0.8
5	0.74 ± 0.06	15.40	0.51	0.94	113.5 ± 1.4
6	2.23 ± 0.06	23.64	0.78	1.20	109.1 ± 0.8
6	2.25 ± 0.07	21.54	0.71	1.46	111.6 ± 0.7
6	2.20 ± 0.03	19.36	0.64	1.77	114.0 ± 1.8
6	1.36 ± 0.02	17.08	0.57	1.40	107.6 ± 0.6
6	0.89 ± 0.01	15.57	0.52	1.11	106.7 ± 0.7
6	5.98 ± 0.34	13.99	0.46	9.19	108.0 ± 0.7
7	5.15 ± 0.16	23.82	0.79	2.73	145.0 ± 1.3
7	3.79 ± 0.14	21.51	0.71	2.46	136.1 ± 0.6
7	2.30 ± 0.02	17.20	0.57	2.34	138.9 ± 1.6
7	1.68 ± 0.01	15.50	0.51	2.10	138.8 ± 0.7
7	1.40 ± 0.01	13.89	0.46	2.18	138.2 ± 1.5
8	6.68 ± 0.23	23.78	0.79	3.56	134.6 ± 3.2
8	5.26 ± 0.19	21.34	0.71	3.48	131.1 ± 2.1
8	2.63 ± 0.06	17.27	0.57	2.65	129.8 ± 1.4
8	2.29 ± 0.03	15.51	0.52	2.86	132.0 ± 1.8
8	1.61 ± 0.02	13.93	0.46	2.50	133.8 ± 1.0
8	1.29 ± 0.02	12.57	0.42	2.45	135.2 ± 2.1
9	3.47 ± 0.12	17.70	0.52	3.79	129.3 ± 2.1
9	2.29 ± 0.07	15.94	0.47	3.09	130.7 ± 1.3
9	1.71 ± 0.03	14.31	0.42	2.86	131.6 ± 0.9

Table S2 Parameters and determined reaction rates of all feeding-step experiments with DMC B.

Experiment	**k_{obs} / 10^{-3} · [1/s]**	**[DMC] / mg/L**	**[ROH] / mol/L**	**k_s·K / 10^{-5} · L^2/(s·mg_{DMC}·mol)**	**T / °C**
1	1.74 ± 0.05	38.14	0.79	5.75	121.5 ± 1.4
1	1.94 ± 0.08	34.06	0.71	8.04	124.1 ± 1.8
1	1.38 ± 0.05	30.49	0.63	7.16	122.1 ± 1.7
1	1.21 ± 0.03	27.38	0.57	7.78	121.2 ± 1.0
1	0.59 ± 0.02	24.64	0.51	4.69	121.0 ± 0.9
1	0.19 ± 0.00	22.10	0.46	1.91	119.8 ± 2.3
2	2.43 ± 0.10	37.58	0.79	8.21	128.6 ± 1.4
2	2.71 ± 0.12	34.17	0.72	11.08	129.2 ± 1.7
2	2.40 ± 0.10	30.33	0.65	12.04	129.9 ± 1.1
2	1.54 ± 0.02	27.24	0.59	9.38	124.6 ± 0.4
2	0.77 ± 0.01	24.51	0.53	5.67	126.1 ± 0.9
2	0.18 ± 0.00	21.94	0.48	1.68	123.5 ± 0.5
3	3.24 ± 0.11	41.17	0.79	9.89	127.5 ± 2.1
3	2.24 ± 0.03	36.98	0.71	8.50	117.0 ± 0.9
3	2.27 ± 0.06	32.93	0.64	10.86	121.3 ± 0.8
3	1.70 ± 0.03	29.60	0.57	10.04	122.3 ± 0.6
3	0.94 ± 0.04	26.62	0.51	6.89	123.0 ± 2.5
3	0.24 ± 0.00	23.92	0.46	2.14	127.8 ± 1.5
4	1.44 ± 0.03	39.70	0.79	4.57	112.7 ± 2.1
4	1.95 ± 0.05	35.84	0.71	7.60	118.1 ± 1.9

4	1.08 ± 0.03	31.72	0.63	5.40	112.3 ± 1.4
4	0.81 ± 0.02	28.46	0.57	5.01	113.5 ± 1.6
4	0.57 ± 0.01	25.61	0.51	4.34	115.4 ± 1.1
5	3.40 ± 0.11	36.30	0.79	11.80	136.3 ± 2.8
5	3.38 ± 0.15	32.36	0.71	14.75	136.0 ± 1.8
5	3.05 ± 0.09	29.12	0.64	16.44	138.3 ± 2.0
5	1.68 ± 0.04	26.18	0.57	11.21	135.7 ± 1.1
5	0.53 ± 0.01	23.47	0.51	4.42	133.5 ± 0.6
6	3.15 ± 0.12	38.90	0.78	10.33	134.0 ± 2.9
6	3.62 ± 0.17	35.12	0.71	14.54	141.0 ± 2.2
6	3.70 ± 0.28	31.62	0.64	18.34	146.1 ± 2.3
6	2.89 ± 0.14	28.42	0.57	17.72	148.1 ± 1.8
6	0.32 ± 0.00	25.52	0.51	2.47	143.9 ± 0.1
7	3.84 ± 0.10	32.80	0.72	16.27	146.1 ± 3.2

Table S3 Parameters and determined reaction rates of all feeding-step experiments with DMC C.

Experiment	**k_{obs} / 10^{-3} · [1/s]**	**[DMC] / mg/L**	**[ROH] / mol/L**	**k_s·K / 10^{-4} · $L^2/(s \cdot mg_{DMC} \cdot mol)$**	**T / °C**
1	14.61	22.39	0.79	8.25	125.6 ± 7.0
1	9.98 ± 1.48	20.26	0.72	6.88	128.5 ± 5.1
1	6.84 ± 0.59	18.19	0.64	5.85	128.4 ± 2.5
1	6.34 ± 0.63	16.31	0.58	6.75	126.0 ± 3.0
1	4.59 ± 0.23	14.62	0.52	6.08	123.1 ± 2.3
1	3.51 ± 0.09	13.13	0.46	5.77	124.9 ± 2.8
1	2.72 ± 0.06	11.81	0.42	5.52	125.9 ± 2.0
2	6.03 ± 0.49	23.19	0.79	3.31	110.4 ± 1.3
2	5.08 ± 0.16	20.72	0.70	3.49	105.3 ± 1.2
2	5.98 ± 0.65	18.78	0.64	5.01	113.9 ± 1.5
2	4.62 ± 0.23	16.86	0.57	4.80	113.7 ± 1.7
2	4.40 ± 0.11	15.18	0.51	5.64	117.0 ± 1.5
2	2.86 ± 0.07	13.65	0.46	4.53	117.1 ± 1.4
2	3.14 ± 0.07	12.30	0.42	6.13	124.1 ± 1.7
3	13.39 ± 0.54	23.37	0.79	7.23	124.3 ± 4.8
3	17.00 ± 0.86	21.08	0.71	11.30	128.6 ± 5.8
3	19.89	19.06	0.65	16.20	132.8 ± 6.5
3	19.77	17.35	0.59	19.40	139.1 ± 7.0
3	13.70 ± 0.19	15.36	0.52	17.10	147.5 ± 6.9
3	8.14 ± 0.01	13.78	0.47	12.70	139.2 ± 6.7
3	6.73 ± 0.15	12.37	0.42	13.00	135.8 ± 4.0

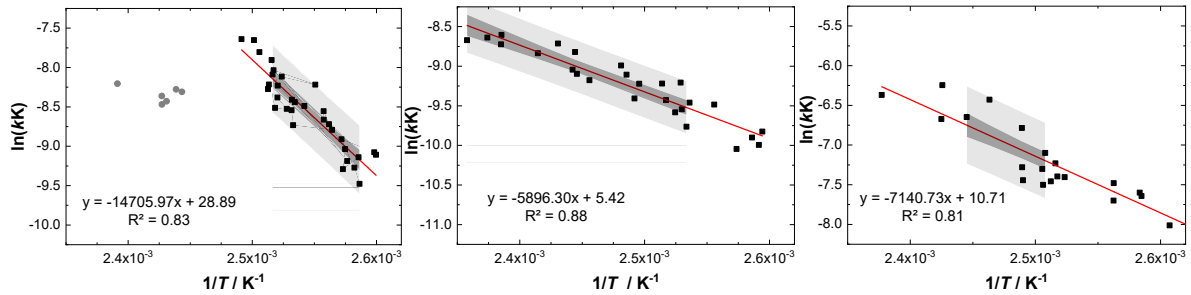

Figure S5 Arrhenius plots of reaction system with from left to right DMC A, DMC B and DMC C showing 95 % prediction band (light grey) and 95 % confidence band (grey).

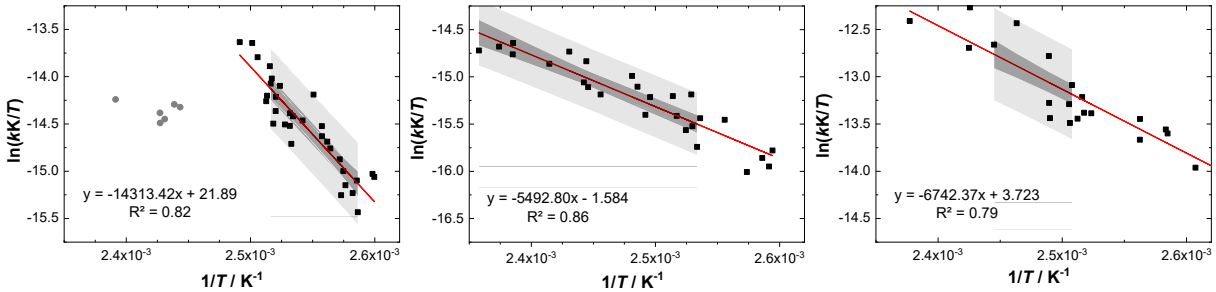

Figure S6 Eyring plots of reaction system with from left to right DMC A, DMC B and DMC C showing 95 % prediction band (light grey) and 95 % confidence band (grey).

Information for Figure 4, S5, S6

DMC/Data	displayed	used in the regression
A	All data	Data T < 130°C
B	Data [ROH] > 0.55 mol/L	Data [ROH] > 0.55 mol/L
C	All data	All data

On the Thiele modulus

The chemical rate of propoxylation would be modified by an effectiveness factor η in case of a porous catalyst. The factor η is defined in terms of the generalized Thiele modulus $\phi(=\frac{V_p}{S}\sqrt{\frac{k}{D_e}}; V_p$: pore volume S: surface area in the pores, D_e: effective diffusion constant near the catalyst; k: rate constant, for a first order reaction) for porous heterogeneous catalysts as $\eta = tanh(\phi)/\phi$. The η would smaller than one for DMC C and B at high $[OH]$ (low mass of PPG at initial pulses). The Thiele modulus would lie inside the range of about 0.2 (no diffusion resistance) and 5 (diffusion limitation). The activation parameter and the observed rate obtained for DMC C and DMC B at high $[OH]$ would thus need to be interpreted as resulting from the dependence of the square root of $k(T) = \sqrt{A} \cdot exp(-E_a/2RT)$ and of (inverse) $D_e(T,\eta)$ [7], [8], [9]. The temperature dependence of the effective diffusion D_e is mainly determined by the temperature dependency of the PO diffusion, *i.e.* in the small temperature range between 370 and 400 K little change in segmental friction factors of the PPG is expected, and thus with activation energy in the range of 20 kJ/mol for the molecular weight range of this study [10]. This leaves the chemical reaction constant with an activation energy for DMC B and C in the range of 120-145 kJ/mol (~ 2 · (49-59) + 20 kJ/mol). These numbers are then very similar to the obtained activation energies of the propoxylation with DMC A.

Diffusion and M_w dependent Viscosity of the reaction mixture at 120 °C

The self-diffusion of PPGs is quite well-documented, in particular at lower temperatures and smaller molecular masses. [10–15] The diffusion constant *D* may be expected to scale exponentially with molecular mass with a mass dependent exponent between -0.6 (M_w(bulk) of ± 2000 Da) to -0.75 (M_w(bulk) of 4200 Da). Diffusion constants extrapolated to higher temperatures give molecular weight dependent values of about 10^{-11} m^2/s. Beyond the critical molecular mass M_c of about 7000 Da, *D* will progressively decrease stronger (exponent reaching down to -2) as entanglements become an issue and mass diffusion becomes more and more determined by reptation [16], [17]. The importance of transient networks between PPGs with molecular weights of this study and at the temperature above 100 °C will be negligible [18], [19].

The diffusion of small molecules in PPGs on the other hand is hardly reported upon, a study with camphor quinone (CQ) showed that the Stokes-Einstein dependence reduces to $D_{SE}(CQ) = a(T/\eta_{visc})^{0.75}$, i.e. the diffusion constant decreases more slowly with viscosity than theoretically. This observation was related to rotation-translational coupling to movements of polymer segments. The viscosity of PPG products at *e.g.* 120 °C scales with an exponent of 1.07 (± 0.03) with the molecular weight (s. suppl between M_w = 2250-16,000 Da). Assuming that similar holds true for PO, leading to $D_{SE}(PO) \sim M_w^{-0.8}$, polymer and monomer will deviate increasingly in diffusivity with increasing molecular mass. This is also the result from calculations on data acquired at 7 °C: correcting for the different radii of gyration of CQ (0.35 nm) and PO (~ 0.1 nm), PO would have about 1.5 times the diffusion constant of PPG with M_w of 2000 Da and 3 times for a PPG of 4000 Da [10], [18], [20]. The viscosity of PPG increases with the weight average mass with exponent of about 1 at the relevant range of temperature and molecular mass (Figure S7; measurements by Dr. Szopinski at our institute).

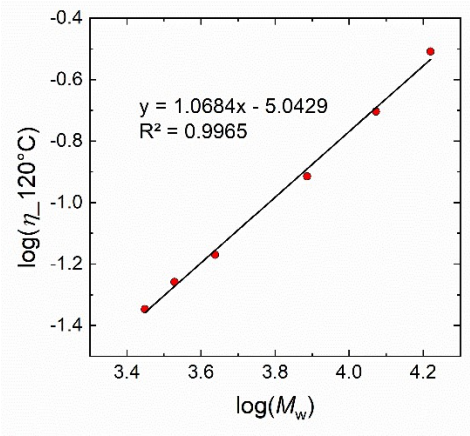

Figure S7 Dynamic viscosity on theoretical weight average molecular weight of PPGs.

On the linearity of $\ln k_sK$ (and $\ln k_sK/T$) and 1/T under diffusion influenced rates

Calculations were carried out on the linearity of "k_sK" in the context of derivation that the following equation holds $-\ln\frac{[OH][DMC]}{k_{obs}(T)} = -\ln\frac{1}{k_sK} = ln(\frac{[OH]}{k_{mPO}(T)} + \frac{1}{k_s(T)K(T)})$, with a 20 kJ/mol activation energy for the diffusion constant, and a negligible contribution from $K(T)$. The Table S4 contains calculation of the k_sK from k_{obs}, where latter is taken from a constant (temperature dependent k_{mPO}) and chemical rate constants k_s with activations energies of 120, 127 and 135 kJ/mol (arbitrary time scale). The Figure S8 shows that in the case with an activation energy of 135 kJ/mol, i.e. with a low rate constant k_s the observable rate k_{obs} are more or less the same. The other case show that k_s and k_{obs} differ, but that a linearity in the function of $\ln k_{obs}$ and 1/T exist. The deviations of the slope between the $\ln k_s$ and $\ln k_{obs}$ vs 1/T are larger at faster rates (black colors, activation energy of 120 °C).

Table S4 Model calculations on a k_{obs} from a chosen mass transfer constant with an activation energy of 20 kJ/mol and a surface reaction constant $k_s(T)$.

	20 kJ/mol	120 kJ/mol		127 kJ/mol		135 kJ/mol	
T / °C	**[OH]/k_{mPO}**	**$k_s(T)$**	**k_s·K**	**$k_s(T)$**	**k_s·K**	**$k_s(T)$**	**k_s·K**
110	18.7	43.1	13.1	4.78	3.81	0.38	0.38
120	22.0	112	18.4	13.2	8.24	1.14	1.08
130	25.6	280	23.4	34.6	14.7	3.18	2.83
140	29.5	665	28.3	86.6	22.0	8.43	6.56

Values for [OH]/k_{mPO} and k_s·K are given in 10^{-6} mol·s/L and 10^{-6} $L^2/(s \cdot mg_{DMC} \cdot mol)$

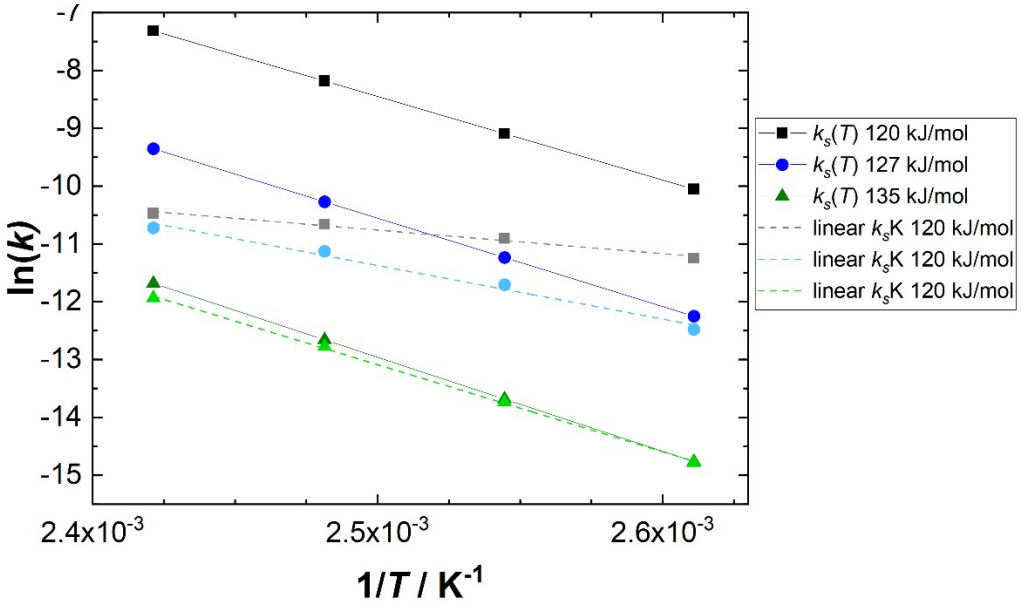

Figure S8 Plot of $\ln k_s$ and $\ln k_{obs}$ vs 1/T for activation energies of 120, 127 and 135 kJ/mol.

Calculations on the action of single DMC crystals

Table S5 Action of single DMC crystals at the first pulse (PPG 2250 mol/L).

	DMC A	DMC B	DMC C
DMC in mg/L	23.8	38.14	23.19
averaged crystal weight 10^{-12} g	0.05 ± 0.02	4 ± 1	0.4 ± 0.1
# crystals/L	$4.8 \cdot 10^{11}$	$1.0 \cdot 10^{10}$	$6.1 \cdot 10^{10}$
10^3 crystals in 10 cm line up	7.8	2.2	3.9
d(cryst-cryst) µm	12.8	45.5	25.6
micro reactor volume in µL	$2.1 \cdot 10^{-6}$	$9.4 \cdot 10^{-5}$	$1.7 \cdot 10^{-5}$
Exponential PO consumption / %	93	58	76
T / °C	124	121	126
k / s^{-1}	$4.33 \cdot 10^{-3}$	$1.74 \cdot 10^{-3}$	$6.03 \cdot 10^{-3}$
TOF pro xtal $1 \cdot 10^{-14}$	1.6	28.6	17.0
Surface 10^{-9} cm^2 per crystal	8.8 ± 3	102 ± 20	32 ± 7
TOF per area of 1 m^2 from crystals	8.5	0.3	3.2
Surface BET /g	107	140	22
Surface of DMC per liter (BET)	2.55	5.34	0.51
total surface of the crystals per L in m^2	0.42	0.11	0.20
ratio surface by BET/crystal calc.	6	50	3
TOF per area of 1 m^2 from BET	29.3	5.6	203.4

Attainable PDIs in the set-up

A broadening of a molecular weight distribution can also originate from the reactor set-up. The viscosity of the PPG is increasing with its molecular weight (thus increasing the Kolmogorov smallest domain). making it also more and more challenging to distribute the PO uniformly into the reaction mixture [21]. This effect could be traced using a propeller stirrer in the reactor while propoxylating with DMC A (Figure S9(l)). Latter stirrer is less effective at higher viscosities than an anchor stirrer. Now a tail of high molecular weight products is readily formed. broadening the PDI (Figure S9(m)). The effects are even more pronounced when the dosing of PO is faster with possible higher local gradients of PO concentration. These results are in accordance with the usual observations [21], [22], [23]. An anchor stirrer is more effective and a narrow distribution is maintained (Figure S9(r)).

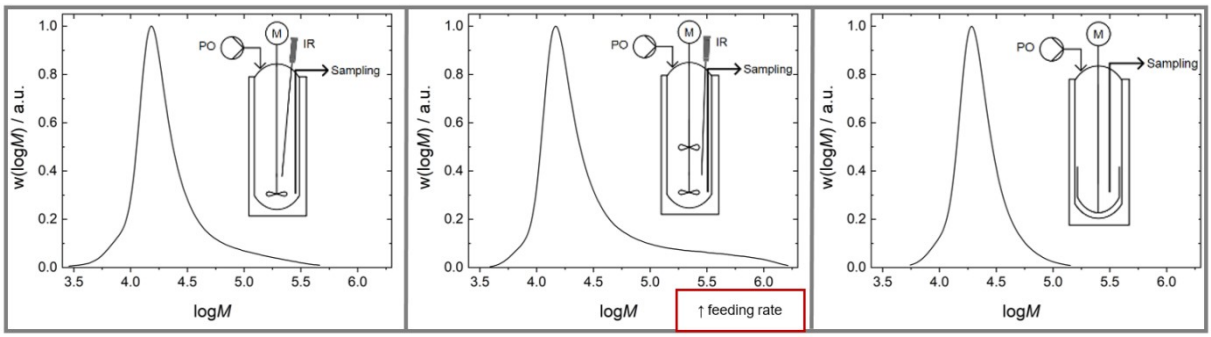

Figure S9 Broadening of the distribution as function of the stirrer geometry or enhanced PO addition rate using DMC A (50 ppm initially) and PPG 2000 as starter at 120 °C.

References

[1] D.F. Mullica, W.O. Milligan, G.W. Beall, W.L. Reeves, Crystal structure of Zn3[Co(CN)6] 2 .12H 2 O, Acta Crystallogr B Struct Sci 34 (1978) 3558–3561.

[2] H.J. Buser, D. Schwarzenbach, W. Petter, A. Ludi, The crystal structure of Prussian Blue: Fe4[Fe(CN)6]3.xH2O, Inorg. Chem. 16 (1977) 2704–2710.

[3] Y. Dienes, W. Leitner, M.G.J. Müller, W.K. Offermans, T. Reier, A. Reinholdt, T.E. Weirich, T.E. Müller, Hybrid sol–gel double metal cyanide catalysts for the copolymerisation of styrene oxide and CO2, Green Chem. 14 (2012) 1168.

[4] F. Herren, P. Fischer, A. Ludi, W. Haelg, Neutron diffraction study of Prussian Blue, Fe4[Fe(CN)6]3.xH2O. Location of water molecules and long-range magnetic order, Inorg. Chem. 19 (1980) 956–959.

[5] J. Rodríguez-Hernández, E. Reguera, E. Lima, J. Balmaseda, R. Martínez-García, H. Yee-Madeira, An atypical coordination in hexacyanometallates: Structure and properties of hexagonal zinc phases, Journal of Physics and Chemistry of Solids 68 (2007) 1630–1642.

[6] M. Avila, L. Reguera, J. Rodríguez-Hernández, J. Balmaseda, E. Reguera, Porous framework of T2[Fe(CN)6]·xH2O with T=Co, Ni, Cu, Zn, and H2 storage, Journal of Solid State Chemistry 181 (2008) 2899–2907.

[7] C.H. Bartholomew, R.J. Farrauto, Fundamentals of Industrial Catalytic Processes, 2nd ed., Hoboken, New Jersey, 2006.

[8] J.M. Thomas, W.J. Thomas, Principles and Practice of Heterogeneous Catalysis, Weinheim, 1997.

[9] E.W. Thiele, Relation between Catalytic Activity and Size of Particle, Ind. Eng. Chem. 31 (1939) 916–920.

[10] A. Schönhals, F. Rittig, J. Kärger, Self-diffusion of poly(propylene glycol) in nanoporous glasses studied by pulsed field gradient NMR: A study of molecular dynamics and surface interactions, The Journal of chemical physics 133 (2010) 94903.

[11] C. León, K.L. Ngai, C.M. Roland, Relationship between the primary and secondary dielectric relaxation processes in propylene glycol and its oligomers, J. Chem. Phys. 110 (1999) 11585–11591.

[12] T. COSGROVE, Self-diffusion, viscosity and spin-spin relaxation in liquid poly(propylene oxide) melts, Polymer 35 (1994) 140–144.

[13] J. Swenson, I. Köper, M.T.F. Telling, Dynamics of propylene glycol and its 7-mer by neutron scattering, J. Chem. Phys. 116 (2002) 5073.

[14] C. Gainaru, W. Hiller, R. Böhmer, A Dielectric Study of Oligo- and Poly(propylene glycol), Macromolecules 43 (2010) 1907–1914.

[15] M. Hofmann, C. Gainaru, B. Cetinkaya, R. Valiullin, N. Fatkullin, E.A. Rössler, Field-Cycling Relaxometry as a Molecular Rheology Technique: Common Analysis of NMR, Shear Modulus and Dielectric Loss Data of Polymers vs Dendrimers, Macromolecules 48 (2015) 7521–7534.

[16] B.A. Smith, E.T. Samulski, L.-P. Yu, M.A. Winnik, Tube Renewal versus Reptation: Polymer Diffusion in Molten Poly(Propylene Oxide), Phys. Rev. Lett. 52 (1984) 45–48.

[17] B.A. Smith, E.T. Samulski, L.P. Yu, M.A. Winnik, Polymer Diffusion in Molten Poly(propylene oxide), Macromolecules 18 (1985) 1901–1905.

[18] M. Appel, G. Fleischer, J. Kärger, I. Chang, F. Fujara, A. Schönhals, Transient entanglement behaviour in a poly(propylene glycole) melt: A field gradient NMR self-diffusion study, Colloid Polym Sci 275 (1997) 187–191.

[19] Gerald Fleischer, Martin Helmstedt, Ingo Alig, Investigations of transient entanglement in oligomeric poly(propylene glycols) with the n.m.r. pulsed field gradient technique and dynamic light scattering, Polymer communications 31 (1990) 409–411.

[20] C.H. Wang, S.S. Gong, Enhancement of tracer diffusion in polypropylene glycol, J. Chem. Phys. 119 (2003) 11445–11450.

[21] J. Hofmann, S. Ehlers, B. Klinksiek, B. Klesczewski, C. Steinlein, L. Obendorf, H. Pielartzik, J.F. Pazos, WO 02/068502, 2002.

[22] J.K. Varghese, D.S. Park, J.Y. Jeon, B.Y. Lee, Double metal cyanide catalyst prepared using H3Co(CN)6 for high carbonate fraction and molecular weight control in carbon dioxide/propylene oxide copolymerization, J. Polym. Sci., Part A: Polym. Chem. 51 (2013) 4811–4818.

[23] R.R. Sharifullin, L.R. Safina, A.S. Biktimerova, N.S. Gabdulkhakova, D.K. Safin, Physicochemical characteristics of polyethers prepared using double metal cyanide catalysts, Catal. Ind. 4 (2012) 243–246.